Solvent Quality Dependent Interactions and Phase Behavior of Polystyrene Particles with Physisorbed PEO−PPO−PEO

ARTICLE *in* LANGMUIR · JANUARY 2002

Impact Factor: 4.46 · DOI: 10.1021/la0110646

2 AUTHORS, INCLUDING:

Peter J. Scales
University of Melbourne
193 PUBLICATIONS **3,908** CITATIONS

Solvent Quality Dependent Interactions and Phase Behavior of Polystyrene Particles with Physisorbed PEO−PPO−PEO

Michael A. Bevan* and Peter J. Scales

Particulate Fluids Processing Centre, University of Melbourne, Victoria, 3010, Australia

Received July 11, 2001. In Final Form: December 12, 2001

This work aims to understand dispersion phase behavior as a function of solvent quality and particle volume fraction for polystyrene (PS) particles stabilized with Pluronic triblock copolymer in 0.5 M NaCl. Measurements of kT interactions between a single colloidal particle and a wall with total internal reflection microscopy (TIRM) indicate a continuous evolution in particle attraction as a function of diminishing solvent quality. The directly measured potential for relatively thin Pluronic layers displays attraction reasonably predicted by Lifshitz theory using only the PS particle properties and neglecting the Pluronic layer properties. The TIRM potential is quantitatively compared with light scattering measurements of temperature-dependent aggregation in dilute, Brownian dispersions for a large range of PS particle radii, a, relative to adsorbed Pluronic layers with thickness, δ. The aggregation behavior is well described as an irreversible flocculation process using the directly measured potential and the Lifshitz prediction for dispersions with $a/\delta > 40$. For dispersions with $a/\delta < 40$, when polymeric interactions dominate, the core PS particle attraction alone is not sufficient to predict the observed aggregation. The directly measured potential and dilute, Brownian aggregation measurements are used to interpret rheological measurements of a fluid−gel transition for high volume fraction dispersions with $a/\delta = 9$. After considering the possible roles of Pluronic desorption and applied shear, a continuum polymeric van der Waals contribution to the net composite interparticle attraction is considered as the source of the observed phase behavior. The polymeric van der Waals contribution for dispersions with small a/δ is addressed with approximate uniform and nonuniform film models. The nonuniform film model predicts sufficient attraction to account for the measured aggregation and fluid−gel data, but the effect of retardation appears to be important for constructing an accurate theoretical phase diagram.

Introduction

The phase behavior of "polymerically" stabilized dispersions is determined by a balance of core particle attractive forces and the forces contributed by an adsorbed or grafted polymer layer. For an adsorbed polymer with a given molecular weight and architecture, the range and magnitude of repulsive or attractive interactions is determined by solvent quality. The term "solvent quality" describes how favorable interactions are between polymer segments and solvent molecules, which changes from "good" to "poor" at the polymer solution Θ temperature. For polymeric stabilization of colloidal dispersions in "good" solvent conditions, interacting adsorbed polymer layers produce repulsion from compression and interpenetration, or alternatively elastic and mixing interactions. When solvent quality changes from "good" to "poor" in a polymerically stabilized dispersion, the polymeric mixing interaction can become attractive and the adsorbed polymer can experience a dimensional collapse that exposes core particle van der Waals attraction. The collapse of adsorbed polymer at the particle surfaces has some analogy with the expansion factor for a bulk solution random coil polymer with diminishing solvent quality.[1] For the poly(ethylene oxide)−water interactions relevant to the present study, solvent quality is determined by thermodynamic factors including temperature,[2,3] pressure,[4] polymer concentration,[5] and the concentration of cosolute molecules,[6,7] which all affect specific molecular interactions. The importance of the specific molecular interactions for polymeric stabilization can be illustrated by the fact that the two most similar polymeric analogues to poly(ethylene oxide)—poly (methylene oxide) and poly (propylene oxide)—are not soluble in water for any thermodynamic conditions and cannot be used to stabilize aqueous colloidal dispersions.[3] Robust polymeric stabilization is ultimately achieved by ensuring that interactions between stabilizing polymer segments and the solvent medium are as favorable as possible at optimal solvent conditions.

Although the solvent quality for a given adsorbed polymer layer in a given solvent clearly depends on specific molecular interactions, the present study is concerned with how the resulting balance of core particle and polymeric interactions contributes to the net continuum interparticle potential and the resulting phase behavior as a function of solvent quality. When determining the interparticle potential for given solvent conditions, the interaction between polymerically stabilized particles depends on the particle size and the adsorbed polymer thickness, which scales the relative core particle and polymeric contributions to the net interaction. For a given polymer layer thickness relative to a core particle radius, altering solvent quality can be used to continuously control

* To whom correspondence should be addressed. E-mail: mabevan@uiuc.edu. Current address: Beckman Institute, University of Illinois, Urbana, IL 61801.

(1) Flory, P. J. *Principles of Polymer Chemistry*; Cornell University Press: Ithica, NY, 1953.
(2) Bailey, F. E.; Callard, R. W. *J. Appl. Polym. Sci.* **1959**, *1*, 56.
(3) Kjellander, R.; Florin, E. *J. Chem. Soc., Faraday Trans. 1* **1981**, *77*, 2053.
(4) Bekiranov, S.; Bruinsma, R.; Pincus, P. *Phys. Rev. E* **1997**, *55*, 577.
(5) Ataman, M. *Colloid Polym. Sci.* **1987**, *265*, 19.
(6) Napper, D. H. *Polymeric Stabilization of Colloidal Dispersions*; Academic Press: New York, 1983.
(7) Florin, E.; Kjellander, R.; Erikson, J. C. *J. Chem. Soc., Faraday Trans. 1* **1984**, *80*, 2889.

10.1021/la0110646 CCC: $22.00
Published on Web 01/26/2002

polymeric interactions relative to core particle van der Waals attraction. Because solvent quality can be used to control the interaction potential between polymer coated particles, it is of significant importance for technological applications that exploit the ability to finely tune dispersion phase behavior. Polymerically stabilized dispersion phase behavior for thick polymer layers relative to the core particle radii is relevant to dispersed microgel particles, nonionic micelles, high-order dendrimers, and proteins, while particles with thin polymer layers are expected to behave as either hard spheres when there is no appreciable attraction, or adhesive spheres when attraction is manipulated continuously via thermodynamic control.

To understand polymerically stabilized dispersion phase behavior, it is critical to have knowledge of the net attraction between the composite particles composed of a core and an adsorbed layer as a function of thermodynamic conditions. Phase behavior of colloidal dispersions refers most generally to both irreversible flocculation for attraction $>10\ kT$ and equilibrium phase transitions for attraction $<5kT$, which can be difficult to distinguish for attraction in the range between $5kT$ and $10kT$. Attraction between polymer coated particles on the order of kT remains poorly understood despite its importance for determining phase behavior in many systems. A poorly understood contribution is the continuum van der Waals attraction between adsorbed polymer layers. The continuum van der Waals interaction between polymerically stabilized particles is always attractive, and depends on the core particles *and* the solvent quality via the density and material dielectric properties of the adsorbed polymer layers.[8−10] A polymeric van der Waals contribution is often cited in the literature as a potential source of unexplained phase behavior, but has not yet been successfully incorporated into the continuum interparticle potential for describing polymerically stabilized dispersion phase behavior. Several approximate theories relevant to the polymeric continuum van der Waals contribution exist, but have seen limited development, probably since the effect is weak for layers in "good" solvent conditions and also because of its apparent unimportance for irreversible flocculation. With a significant dimensional collapse of an adsorbed polymer layer due to diminishing solvent quality, the increasing density of the layer can be expected to have an increasingly important effect on the net van der Waals attraction, and as a result be a critical factor for determining both irreversible flocculation and equilibrium phase behavior. While solvent quality dependent polymeric interactions have been measured in the literature,[11,12] these are generally for strong interactions much greater than $10\ kT$, which are not directly relevant to phase transitions. Although phase diagrams for polymerically stabilized dispersions can be created using model pair interactions, the attraction is typically a fitting parameter that does not necessarily lend direct insight into the underlying physics, and in particular the effects of adsorbed layers on the net continuum van der Waals attraction.

In the present study, we attempt to understand the temperature and volume fraction dependent ($T-\phi$) phase behavior of poly(styrene) (PS) particles with physisorbed Pluronic (PEO−PPO−PEO) layers. Previous measurements are briefly reviewed for the forces and hydrodynamic interactions between PS surfaces bearing adsorbed Pluronic layers as a function of temperature obtained using total internal reflection microscopy (TIRM).[9] By using TIRM, which measures interaction energies on the order of kT,[13] it is possible to consider interactions relevant to phase behavior in PS/Pluronic dispersions. These direct measurements of infinitely dilute, Brownian interactions are then quantitatively compared with phase behavior in PS/Pluronic dispersions. Light scattering is used to measure the temperature dependent phase behavior in dilute, Brownian dispersions for a range of PS particle sizes relative to Pluronic layer thicknesses. By exploring a large range of relative particle sizes and layer thicknesses, data is generated to quantify the relative contributions of the core particle and polymeric layer as a function of solvent quality. Using the directly measured TIRM potential and the aggregation measurements as a basis for understanding dilute behavior, rheological measurements are then employed to explore phase behavior in optically dense concentrated PS/Pluronic dispersions. In these measurements, the possible roles of Pluronic desorption and mechanical effects of shear are considered when interpreting the resulting temperature and volume fraction dependent fluid−gel phase behavior. When considering all of the measurements in this paper it appears that a solvent quality dependent continuum polymeric van der Waals attraction is the most likely mechanism for explaining phase behavior in dispersions with Pluronic layers that are thick compared to the PS particle radii. Two approximate models are used to explore limiting cases where the adsorbed Pluronic is shown to contribute significantly to the net attraction, which suggest future work to generate more exact models. This work provides an initial attempt to quantitatively link direct microscopic measurements of the interparticle potential and theories for a continuum polymeric attraction with macroscopic phase behavior and associated rheological transitions in polymerically stabilized dispersions.

Experimental Section

Materials. Polystyrene (PS) particles used in the high volume fraction rheology experiments were prepared using a literature surfactant free emulsion polymerization method.[14] Only one particle size was used in these studies, which was measured with dynamic and static light scattering to have a mean diameter of 360 nm with a polydispersity index of 1.08. The polymer adsorbed to the PS particles was F108 Pluronic triblock copolymer (poly(ethylene oxide)/poly(propylene oxide)/poly(ethylene oxide), or PEO−PPO−PEO) supplied by BASF Wyandotte Corporation. Although Pluronic is known to be polydisperse, the average molecular weight of the F108 Pluronic is reported as 14000 with a PEO molecular weight of 10750 and a PPO molecular weight of 3250.[15] These molecular weights correspond to the F108 Pluronic having an anchor block of 56 PPO monomer units and two buoy blocks of 122 PEO monomer units. All solutions used in these experiments were prepared with double deionized water. Since PEO is known to degrade by oxidation in aqueous solutions,[16] experiments were performed within 2 weeks of solution preparation.

Methods. High volume fraction PS particle dispersions were polymerically stabilized by slow addition of 1000 ppm Pluronic solution to dispersions of less than 10% volume fraction over a 24 h period while stirring. Centrifugation was used to remove

(8) Parsegian, V. A. *J. Colloid Interface Sci.* **1975**, *51*, 543.
(9) Bevan, M. A.; Prieve, D. C. *Langmuir* **2000**, *16*, 9274.
(10) Prieve, D. C.; Russel, W. B. *J. Colloid Interface Sci.* **1988**, *125*, 1.
(11) Almog, Y.; Klein, J. *J. Colloid Interface Sci.* **1985**, *106*, 33.
(12) Israelachvili, J. N.; Tirrell, M.; Klein, J.; Almog, Y. *Macromolecules* **1984**, *17*, 204.
(13) Prieve, D. C. *Adv. Colloid Interface Sci.* **1999**, *82*, 93.
(14) Goodwin, J. W.; Hearn, J.; Ho, C. C.; Ottewill, R. H. *Colloid Polym. Sci.* **1974**, *252*, 464.
(15) Baker, J. A.; Berg, J. C. *Langmuir* **1988**, *4*, 1055.
(16) Bailey, F. E., Koleske, J. V., Eds. *Aklyene Oxides and their Polymers*; Marcel Dekker: New York, 1990; Vol. 35, p 261.

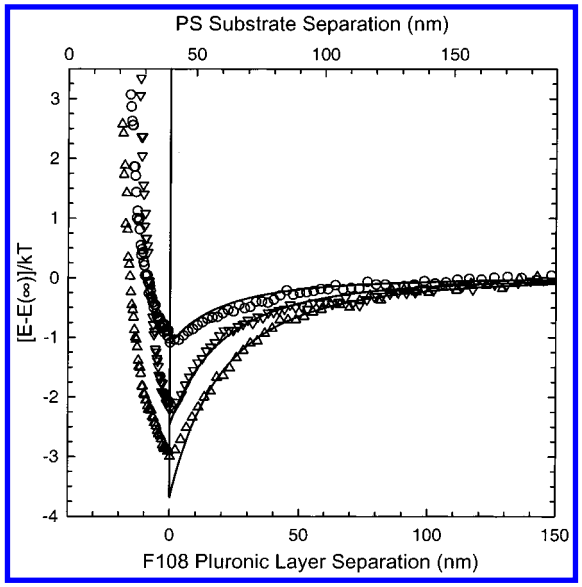

Figure 1. Potential energy profiles for polystyrene particles polymerically levitated with F108 Pluronic with nominal sizes of 1.9 (○), 4.2 (▽), and 6.3 (△) μm. These data are shown with the gravitational contribution subtracted and theoretical curves (—) using eq 1 (partially replotted from ref 9).

excess bulk polymer and to replace the supernatant with 0.5 M NaCl to suppress electrostatic interactions. This washing step was repeated until dispersions displayed an unchanging shear dependent viscosity. Once the Pluronic stabilized PS particle dispersions were adequately cleaned, centrifugation was used to prepare 2 stock dispersions at the lowest and highest volume fractions. All other dispersions used in this study were prepared by mixing these two stock batches in different proportions. The core particle volume fraction in the two stock batches was determined gravimetrically using the density of PS as 1.055 kg/m^3, which resulted in the same volume fraction whether the adsorbed polymer layer density was included or not.

Several techniques were used to probe the rheological properties of these relatively high volume fraction dispersions. The viscosity of dispersions with effective volume fractions less than 12% were measured using a Schott Gerate capillary viscometer with automated dilutions. Each dilution was measured 10 times and each experiment was repeated twice to check reproducibility. The steady and oscillatory shear experiments were performed using a CarriMed cone and plate rheometer with a low inertia acrylic cone with no protective silicone oil for measurements at 20 °C. For experiments at elevated temperatures, a temperature controlled plate was used with the cone and plate geometry, and the sample was protected with a cover, solvent trap, and low viscosity silicone oil to seal the system. Various heating rates were checked in each experiment to ensure that a reasonable steady state was achieved at each temperature. Steady shear experiments were performed in an equilibrium mode to ensure a steady rate was achieved for each applied stress. Oscillatory shear measurements were performed with a strain amplitude of 0.005 at a frequency of 3 Hz to ensure linear viscoelastic measurements for fluid and gelled PS/Pluronic dispersions at all temperatures.

Results and Discussion

Dilute, Brownian PS/Pluronic Interactions, and Phase Behavior ($a/\delta_0 = 4-500$, $T = 25-90$ °C, $\phi = 0-10^{-2}$, Pe = 0). To compare macroscopic dispersion phase behavior with the microscopic interparticle potential, Figure 1 shows direct TIRM[13] measurements of potential energy profiles. These measurements are for single, Brownian PS particles interacting with PS spin coated microscope slides with both surfaces bearing adsorbed F108 Pluronic layers. The profiles are for 1.9, 4.2, and 6.3 μm PS particles in 0.5 M NaCl used to suppress electrostatic interactions. These measurements were performed at 25 °C which corresponds to near optimal solvent conditions for the PEO block of the Pluronic.[7,17] Although these profiles are discussed extensively in a previous manuscript,[9] the data are replotted here with a modified theoretical representation in eq 1 to quantitatively interpret macroscopic phase behavior measurements in the present work. Equation 1 is represented by a "hard wall" repulsive term and a continuum van der Waals attraction term. The interaction potential in eq 1 is given as a function of particle size, a, temperature-dependent adsorbed polymer layer thickness, $\delta(T)$, and the separation between PS substrate surfaces, h. The constant C has an arbitrary large value here, and H is the Heaviside step function. The screened and retarded half space Hamaker function, $A_{121}(l)$, is calculated with no adjustable parameters[18] and is given generally by the empirical fit in eq 2 with a and h having units of nanometers and $A_{121}(l)$ having units of kT. For the theoretical attraction shown in Figure 1, $A_{121}(l)$ is calculated ignoring the dielectric properties of the Pluronic layer and treating the layer using water properties instead of PEO/PPO properties. This is the conventional model for polymeric stabilization. The potential in eq 1 is reported for particle−particle interactions; however, particle-wall interactions in Figure 1 are accurately predicted by replacing the radius, a, with the particle diameter, $2a$.

$$E(h,a,\delta,T) = CH[h - 2\delta(T)] - \frac{a}{12}\int_h^\infty \frac{A_{121}(l)}{l^2}\,\mathrm{d}l \quad (1)$$

$$(1/12)\int_h^\infty \frac{A_{121}(l)}{kTl^2}\,\mathrm{d}l = \frac{8.26\times10^4 + 6.08\cdot10^3 h - 9.48h^2 - 0.0068h^3}{1 - 4.50\times10^5 h - 9.53\times10^4 h^2 - 6.23\times10^3 h^3} \quad (2)$$

It is critical to note that the good agreement observed between the measured attraction and the prediction from eq 1 is somewhat misleading. The apparent agreement actually arises from two compensating effects; the bare PS van der Waals attraction is weakened due to surface roughness,[18] but the adsorbed Pluronic strengthens the van der Waals attraction relative to PS substrate separation.[9] The net result is somewhat coincidental agreement between the measured attraction and the prediction from eq 1 neglecting Pluronic dielectric properties. However, for the near optimal solvent conditions and large particle radii relative to Pluronic thickness ($a/\delta_0 \gg 1$) in Figure 1, the effects of adsorbed polymer and surface roughness on the net attraction are negligible for dispersion phase behavior.

With increasing temperature and diminishing solvent quality for the Pluronic layer, a dimensional collapse of the adsorbed polymer will increase its density and its contribution to the net continuum van der Waals attraction. Figure 2 shows the temperature-dependent layer thickness, δ(T), previously measured using TIRM[9] and interpreted from stability data,[9,19] with a new fit given by eq 3. The thickness of the F108 Pluronic layer in Figure 2 relative to its initial and final thickness given by δ^* generalizes these results for other Pluronic molecular

(17) Chew, B.; Couper, A. *J. Chem. Soc., Faraday Trans. 1* **1973**, *72*, 382.
(18) Bevan, M. A.; Prieve, D. C. *Langmuir* **1999**, *15*, 7925.
(19) Bevan, M. A.; Prieve, D. C. In *Polymers in Particulate Systems: Properties and Applications*; Hackley, V. A., Somasundran, P., Lewis, J. A., Eds.; Marcel Dekker: New York, 2001; Vol. 104.

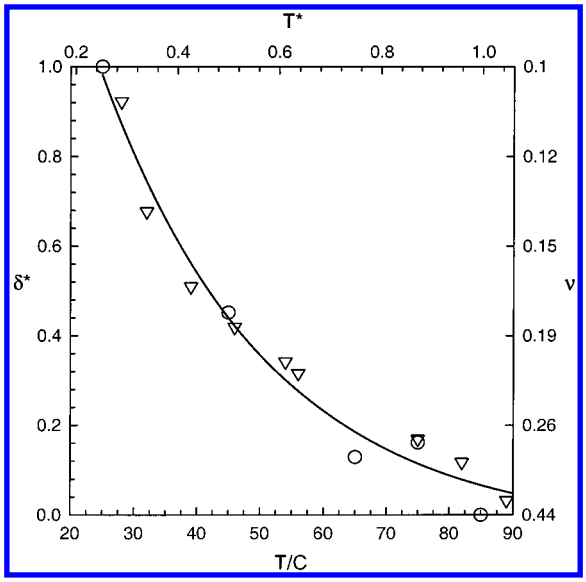

Figure 2. Nondimensional polymer layer thickness δ^* (eq 3) as a function of temperature (°C) from TIRM measurements (○), and inferred from particle−aggregate T_C data in Figure 3 (▽). Scales are also shown for the nondimensional temperature T_C^* (eq 4) and average polymer layer concentration ν (eq 5) (partially replotted from ref 19).

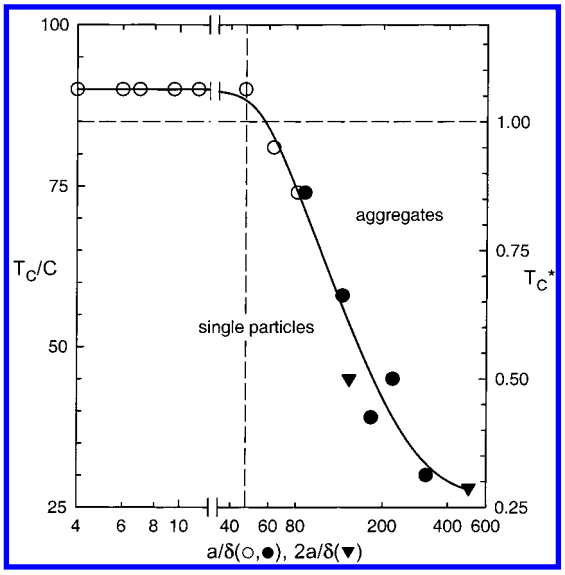

Figure 3. Particle−aggregate temperature data T_C (°C) as a function of a/δ for particle−particle (○) interactions or $2a/\delta$ for particle−wall interactions (▽). Transitions that were reversible with a return to good solvent conditions have open symbols, and irreversible transitions have filled symbols. A scale is also shown for the nondimensional temperature T^* (eq 4) (partially replotted from ref 19).

weights and thicknesses probed in previous studies.[19,20] For F108 Pluronic, the temperature-dependent layer thickness is given by eq 3 with $\delta_0 = 20$ nm at 25 °C and $\delta_f = 4.5$ nm at 90 °C. The layer thickness is reported in terms of a nondimensional temperature scale, T^*, given by eq 4 which varies from $T^* = 0 \rightarrow 1$ for $T = \Theta_L \rightarrow \Theta_H$. This scaling relates the absolute temperature to critical temperatures for PEO in 0.5 M NaCl at $T = \Theta_H \cong 85$ °C[7] and $T = \Theta_L \cong 5$ °C,[17] and generalizes eq 1 for comparison with other polymerically stabilized dispersions and polymer solution phase behavior.

$$\delta^* \equiv \frac{\delta(T^*) - \delta_f}{\delta_0 - \delta_f} = 5.6 \exp[-\exp(1.6T^* + 0.15)] \quad (3)$$

$$T^* \equiv \frac{T - \Theta_L}{\Theta_H - \Theta_L} \quad (4)$$

The change in the average adsorbed Pluronic concentration at the PS particle surfaces with increasing temperature and diminishing solvent quality is shown in Figure 2 and is given by eq 5. The average concentration, ν, of the adsorbed Pluronic is calculated using the bulk density of PEO as $\rho_{PEO} = 1$ kg/m^3 and a conservative low estimate of the adsorbed amount as $\Gamma = 2$ mg/m^2.[20,21] This temperature dependent Pluronic layer concentration is qualitatively similar to literature SAXS and SANS studies of the same effect for PNIPAM grafted to PS particles.[22] The average Pluronic concentration in the layer for near optimal solvent conditions at 25 °C is $\nu = 0.1$, indicating a layer with mostly water properties. This is consistent with the attraction in Figure 1 being reasonably predicted by eq 1 ignoring the polymer dielectric properties.

$$\nu(T^*) = \Gamma/[\delta(T^*)\rho_{PEO}] \quad (5)$$

As the temperature increases, the Pluronic thickness decreases to $\delta_f = 4.5$ nm at 90 °C, and its concentration increases to $\nu = 0.44$ at 90 °C. The increased density of Pluronic causes the layer to have dielectric properties less like water, which will cause the Pluronic continuum van der Waals contribution to be increased compared to a layer with only water properties. In the event of a complete collapse to $\nu = 1$, or $\delta_f = \Gamma/\rho_{PEO}$, the Pluronic layer would contribute its maximum van der Waals attraction. At a given solvent condition, the relative size of the core PS particle and the Pluronic layer, characterized by a/δ_0, determines the contributions of each material to the net composite particle attraction. For the relatively thin polymer layers in Figure 1 with $2a/\delta_0 = 100-300$ (the "2" scales the particle-wall interaction), the large core PS particle dominates the net attraction, or the polymeric van der Waals contribution is small compared to the particle contribution. Although the solvent quality dependent Pluronic layer contribution is expected to be relatively unimportant for large a/δ_0, changing the Pluronic layer thickness and concentration when adsorbed to a relatively small PS core is potentially critical for small a/δ_0 composite PS/Pluronic particle attraction.

To probe conditions where the Pluronic temperature dependent collapse and resulting van der Waals contribution more significantly influence stability and phase behavior, Figure 3 reports measurements of a temperature-dependent particle−aggregate transition, T_C, for composite PS/Pluronic particles with $a/\delta_0 = 4-500$ (reconstructed from refs 19and 20). Open symbols indicate redispersion upon cooling to good solvent conditions, and filled symbols indicate that redispersion did not occur with cooling. These data were obtained for PS particles with radii between 70 nm and 1 μm with adsorbed P85 ($\delta_0 =$ 3 nm[15]) and F108 Pluronics. Temperature instabilities measured with TIRM for levitated 10 μm and 2.8 μm PS particles with F108 Pluronic layers are also reported in Figure 3 as a function of $2a/\delta_0$. Equation 6 is an empirical fit to the data shown as the solid line in Figure 3.

(20) Bevan, M. Ph.D. Dissertation, Carnegie Mellon University, 1999.
(21) Stenkamp, V. S.; Berg, J. C. *Langmuir* **1997**, *13*, 3827.
(22) Seelenmeyer, S.; Deike, I.; Rosenfeldt, S.; Norhausen, C.; Dingenouts, N.; Ballauff, M.; Narayanan, T.; Lindner, P. *J. Chem. Phys.* **2001**, *114*, 10471.

$$T^*_C(a,\delta_0) \equiv \frac{T_C(a,\delta_0) - \Theta_L}{\Theta_H - \Theta_L} = 0.27 + 0.79[1 + \exp(0.15(a/\delta_0) - 7.6)]^{-0.066} \quad (6)$$

The relative contributions of the core PS particle and the Pluronic layer as a function of solvent quality are critical for determining the observed temperature-dependent aggregation. For PS/Pluronic particles with $a/\delta_0 > 85$, the T_C values are quantitatively predicted by eq 1 using water dielectric properties for the Pluronic and treating the aggregation as irreversible flocculation with a critical interparticle attraction of $-7kT$. In the range $40 < a/\delta_0 < 85$, eq 1 continues to accurately describes the aggregation as irreversible flocculation, but the breakup of aggregates with a return to good solvent conditions suggests the increasing importance of polymeric interactions relative to core particle van der Waals attraction. For $a/\delta_0 < 40$, the T_C values cannot be predicted using eq 1 ignoring the Pluronic properties and modeling the transition as irreversible flocculation. It is possible that attraction $<5kT$ produces the observed aggregation due to an equilibrium phase transition, although the measured aggregation kinetics for all of the data in Figure 3 are characteristic of irreversible flocculation (at least for 1 aggregation cycle).[19,20] It is more likely that aggregation for the relatively thick Pluronic layers with $a/\delta_0 < 40$ indicates the increased role of polymeric attraction. Although it is not unexpected that polymeric attraction contributes to particle aggregation for thick Pluronic layers near $T^* = 1$, it is important to consider the source of the polymeric attraction.

Accurate modeling of aggregation for thick polymer layer dispersions requires consideration of both molecular polymeric "mixing" attraction and continuum polymeric van der Waals attraction. These effects are incorporated into eq 1 by requiring the hard wall repulsive term to become attractive at $T^* \approx 1$ and including the Pluronic dielectric profile when calculating the retarded half space Hamaker function $A_{13231}(l)$. Most studies interpret measurements of polymeric attraction for diminished solvent conditions in the vicinity of $T^* = 1$ as a purely polymeric "mixing" interaction, which has been studied extensively in theory and experiment.[23] A few theoretical investigations have suggested the effects of uniform[24] and nonuniform[8,25] films on van der Waals interactions, and only the experimental studies of Israelachvili et al.[26] and Bevan et al.[9] have measured and identified the effects of films on continuum van der Waals attraction. Because the aggregation temperature in Figure 3 is greater than the PEO Θ_H temperature ($T_C > T^*$) for $a/\delta_0 < 40$, it is reasonable to suggest the source of attraction in the present case is due primarily to polymer mixing. A subtle factor that suggests the importance of a long range continuum attraction over a "mixing" attraction at polymer contact is the following: aggregation is only kinetically possible when a long-range attraction overcomes a divergent interparticle hydrodynamic repulsion that opposes bringing particle surfaces into contact.[27] The indirect nature of the measurements presented in Figure 3 do not provide enough information to quantitatively distinguish the two sources of polymeric attraction. Although the potential in eq 1 is quantitatively accurate with no adjustable or fitted parameters for PS/Pluronic composite particles with $a/\delta_0 > 40$, it is important to understand the attractive mechanisms controlling phase behavior for $a/\delta_0 < 40$.

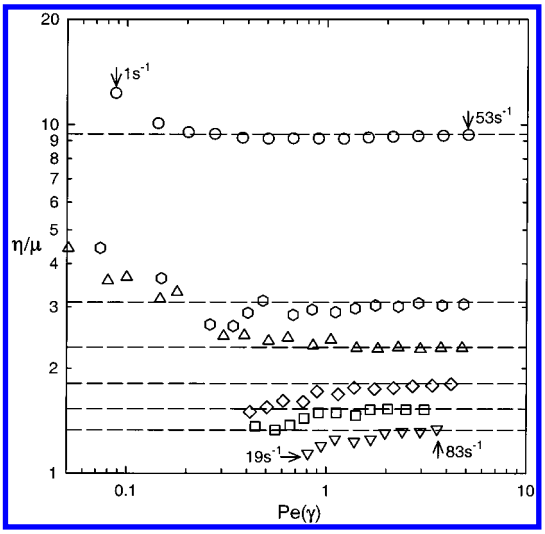

Figure 4. Normalized dispersion viscosity η/μ as a function of Peclet number for effective volume fractions (eq 7) of 0.119, 0.162, 0.194, 0.227, 0.2589, and 0.367. Several absolute shear rates are also indicated.

Concentrated PS/Pluronic Dispersion Rheology and Phase Behavior ($a/\delta_0 = 10$, $T = 25-90$ °C, $\phi = 0.02-0.4$, $Pe = 0.1-1$). To further explore solvent quality dependent polymeric attraction for PS/Pluronic particles with $a/\delta_0 < 40$, the remainder of this paper probes high volume fraction phase behavior, which is sensitive to weak attraction less than $5kT$.[28] In particular, temperature-dependent rheological transitions are measured for concentrated dispersions of 360 nm PS particles with adsorbed F108 Pluronic having $a/\delta_0 = 9$. Although the micron sized PS particle-wall interactions in Figure 1 display attractive minima on the order of kT for near optimal solvent conditions, the size dependence in eq 1 indicates that attraction vanishes for submicron PS particle−particle interactions with adsorbed F108 Pluronic at 25 °C. For these 360 nm PS particles with 20 nm Pluronic layers, neglecting the Pluronic dielectric properties in the van der Waals term in eq 1 predicts attraction less than $1kT$ up to $T^* = 0.9$ and less than $1.3kT$ up to $T^* = 1.05$. Any phase transitions observed below $T^* \cong 1$ are therefore indicative of polymeric van der Waals attraction since a polymeric mixing attraction is not expected for these favorable solvent conditions.

Figure 4 displays viscosity as function of shear rate for 360 nm PS particles with adsorbed F108 Pluronic at 25 °C ($a/\delta_0 = 9$) with effective volume fractions of $\phi_{eff} = 0.119$, 0.162, 0.194, 0.227, 0.2589, 0.302, and 0.367. Reporting the results in terms of effective volume fraction using eq 7 assumes the composite PS/Pluronic particles can be treated as effective hard spheres. The profiles in Figure 1 and eq 1 indicate this is reasonable since the adsorbed Pluronic layers are hydrodynamically impermeable and produce strong osmotic repsulsion,[9,29] at least for Brownian collisions. The Peclet number, Pe, given by eq 8 is used in Figure 4 to scale the applied shear rate with the particle Brownian diffusion rate. This scaling indicates the extent

(23) Insergent, K.; Klein, J.; Pincus, P. *Macromolecules* **1986**, *19*, 1374.
(24) Vold, M. J. *J. Colloid Sci.* **1961**, *16*, 1.
(25) Vincent, B. *J. Colloid Interface Sci.* **1973**, *42*, 270.
(26) Israelachvili, J. N.; Tabor, F. R. S. D. *Proc. R. Soc. London A* **1972**, *331*, 19.
(27) Honig, E. P.; Roebersen, G. J.; Wiersema, P. H. *J. Colloid Interface Sci.* **1971**, *36*, 97.
(28) Russel, W. B.; Saville, D. A.; Schowalter, W. R. *Colloidal Dispersions*; Cambridge University Press: New York, 1989.
(29) Bevan, M. A.; Prieve, D. C. *J. Chem. Phys.* **2000**, *113*, 1228.

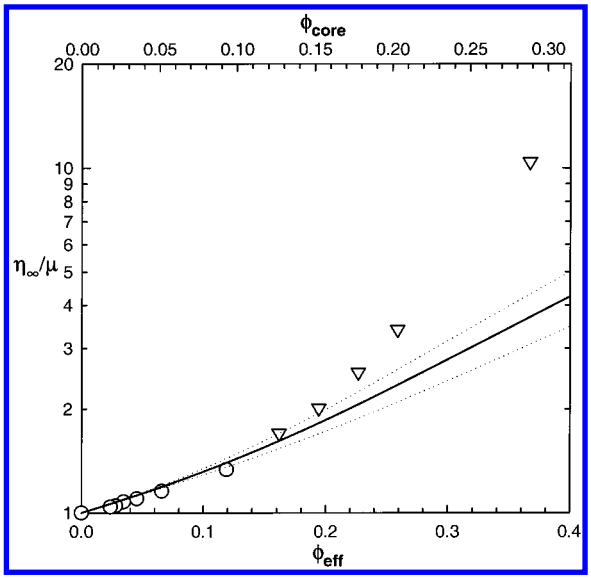

Figure 5. High shear viscosity from capillary (○) and cone-and-plate measurements (▽) for effective volume fractions (eq 7) of 0.119, 0.162, 0.194, 0.227, 0.2589, and 0.367. The solid line and dotted error lines represents literature hard sphere data given by eq 9.[31] A scale is also shown for the core particle volume fraction.

to which applied shear perturbs Brownian particle interactions and structure. The Pe number is determined using the Stokes−Einstein diffusion coefficient, D_0, modified by $f(\phi)$[30] to account for increasingly hindered particle diffusion with increasing particle volume fraction. The aqueous 0.5 M NaCl medium viscosity and the shear rate are given by μ and γ in eq 8.

$$\phi_{eff}(T^*) = \phi_{core}(1 + \delta(T^*)/a_{core})^3 \quad (7)$$

$$\mathrm{Pe} = \frac{a^2/D_S(\phi)}{\dot{\gamma}^{-1}} = \frac{a^2\dot{\gamma}}{D_0 f(\phi)} = \frac{\mu a^3 \dot{\gamma}}{kT(1 - 1.56\phi)(1 - 0.27\phi)} \quad (8)$$

For shear rates where reliable data was obtained in Figure 4, the viscosity displays some shear thinning behavior for $\phi_{eff} > 0.2$, but is independent of Pe for $\phi_{eff} < 0.2$. For the range of shear rates measured with Pe = 0.1−5 in Figure 4, the degree of shear thinning measured for the PS/Pluronic dispersions is similar to hard spheres.[31] The observed shear thinning for $\phi_{eff} > 0.2$ occurs for Pe ≈ 0.1 near the low stress limit of the rheometer so that plateau values of low shear limiting viscosities, η_0, are not reported for these dispersions. As a result, it was not possible to assess the role of weak particle attraction on the low shear viscosity for the dispersions in Figure 4. The relative shear independence of the data for Pe > 1 suggests the measured viscosities correspond to high shear limiting values, η_∞. Figure 5 shows values of η_∞ determined from Figure 4 on a log scale as a function of ϕ_{eff} and ϕ_{core}. The solid line and dotted error lines show literature data for η_∞ measured for index matched hard sphere dispersions given by eq 9.[31]

$$\frac{\eta_\infty}{\mu} = 1 + 2.5\phi_{eff} + (4 \pm 2)\phi_{eff}^2 + (25 \pm 7)\phi_{eff}^3 \quad (9)$$

Agreement is observed between the PS/Pluronic data and literature hard sphere data given by eq 9 up to ϕ_{eff} ≈ 0.2 in Figure 5. For $\phi_{eff} > 0.2$, a trend for increasingly greater than hard sphere viscosities is apparent in Figure 5, which suggests an increasing interparticle attraction. For measurements of a PS/Pluronic dispersion with ϕ_{eff} = 0.41 not shown in Figures 4 and 5, the viscosity was initially $\eta/\mu \approx 20$ for 0.1 < Pe < 1, but for Pe > 1 the viscosity became immeasurably high at 20 °C appearing to indicate a fluid−gel transition. The transition was qualitatively reversible from macroscopic observation of the sample, although identical equilibrium shear curves for increasing and decreasing shear rate were not obtained, possibly due to slow redispersion. The fluid−gel transition for $\phi_{eff} = 0.41$ and the increasingly greater than hard sphere viscosities for $\phi_{eff} > 0.2$ suggest either a volume fraction dependent interparticle attraction or a volume fraction independent attraction that is rheologically significant for increased particle number density and many body interactions.

Compression of adsorbed polymeric layers with increasing ϕ_{eff} has been previously suggested as a potential reason for polymerically stabilized dispersion viscosities deviating from hard sphere behavior.[28] For thick polymer layer dispersions, measurements of less than hard sphere viscosities were interpreted as a reduction of the adsorbed layer and net particle size with increasing volume fraction. In contrast, greater than hard sphere viscosities measured for thin polymer layer dispersions were suggested to occur from core particle van der Waals attraction exposed by a reduction in polymer thickness. Since the PS/Pluronic viscosities in Figure 5 are for thick polymer layers, the viscosity might be expected to decrease due to an effective particle size decrease, but the increased viscosity instead suggests an attractive contribution. Because the temperatures correspond to good solvent conditions at 25 °C in Figures 4 and 5, a polymeric mixing attraction is not expected. Neglecting the Pluronic layer properties, eq 1 indicates that 20 nm F108 Pluronic layers would have to collapse to 6 nm at 25 °C to expose 1kT of the 360 nm core PS particle attraction, which seems unlikely. However, an increased continuum polymeric attraction would also occur as a result of a volume fraction dependent Pluronic collapse and an associated layer density increase. It is difficult to quantify and determine the source of particle attraction from the viscosity measurements in Figures 4 and 5. However, these good solvent measurements do provide a basis for evaluating the effect of diminishing solvent quality in PS/Pluronic concentrated dispersion rheology.

For the same dispersions used in Figures 4 and 5, Figure 6 now displays the reduced viscosity at a fixed shear stress as a function of increasing temperature, or diminishing solvent quality. The resulting shear rate for all volume fractions was around Pe ≈ 1. For each effective volume fraction, the reduced viscosity, $\eta_r(T)$, reported in Figure 6 is calculated using eq 10 with the measured viscosity at 20 °C, η(20 °C), and the measured temperature dependence of the aqueous 0.5 M NaCl viscosity, $\mu_w(T)/\mu_w$(20 °C). The solid curve in Figure 6 is calculated using eq 11 for $\phi_{eff} = 0.16$, which uses the volume fraction dependent viscosity for hard spheres from eqs 7 and 9 and tabulated data for $\mu_w(T)/\mu_w$(20 °C).[32]

(30) Pearson, D. S.; Shikata, T. *J. Rheol.* **1994**, *38*, 601.
(31) Kruif, C. G. d.; Iersel, E. M. F. v.; Vrij, A.; Russel, W. B. *J. Chem. Phys.* **1985**, *83*, 4717.
(32) Lide, D. R., Ed. *CRC Handbook of Chemistry and Physics*; CRC Press: New York, 2000; Vol. 80.

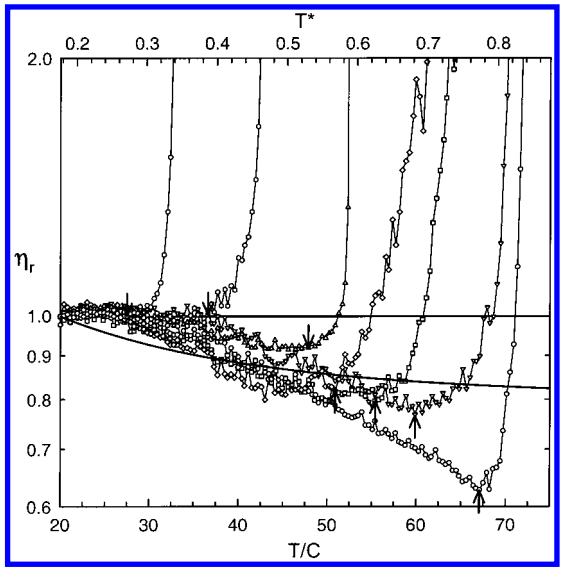

Figure 6. Reduced viscosity η_r (eqs 10 and 11) as a function of temperature (°C) for effective volume fractions (eq 7) of 0.119, 0.162, 0.194, 0.227, 0.2589, 0.302, and 0.367. A scale is also shown for the nondimensional temperature T^* (eq 4). Arrows (↑) indicate values for T_C^* reported in Figure 9.

$$\eta_r(T) = \frac{\eta(T)/\eta(20\ °C)}{\mu_w(T)/\mu_w(20\ °C)} \tag{10}$$

$$\eta_r(T) = \frac{\eta\{\phi_{eff}[\delta(T)]\}/\eta\{\phi_{eff}[\delta(20C)]\}}{10^{\{[1.3272(20-T)\ -\ 0.001053(T-20)^2][T+105]^{-1}\}}} \tag{11}$$

For each dispersion measured in Figure 6, a transition from decreasing to increasing dispersion viscosity with increasing temperature is indicated by an arrow on each curve. This transition from a viscous fluid to an elastic solid is considered to be a "fluid−gel" transition since a gel phase is the most likely elastic particle structure for $\phi_{eff} = 0.12-0.37$, although no direct structural measurements were performed. The transition temperatures indicated by the arrows in Figure 6 are summarized in Figure 9, including the $\phi_{eff} = 0.41$ transition at 20 °C for Pe ≈ 1 mentioned in the discussion of Figures 4 and 5. Similar to the $\phi_{eff} = 0.41$ transition, the transitions measured in Figure 6 were also qualitatively reversible from macroscopic observation, although quantitatively reversible viscosity−temperature curves were not obtained.

The initial decrease in the reduced viscosities in Figure 6 to values less than unity, $\eta_r(T) < 1$, is consistent with a temperature-dependent Pluronic collapse and an associated decrease in effective particle size and volume fraction. The solid line shown in Figure 6, calculated using eq 11 for $\phi_{eff} = 0.16$ with the polymer collapse in eq 3, can be seen to qualitatively capture the decreasing viscosity prior to the transition. Although only shown for $\phi_{eff} = 0.16$, eq 11 produces qualitative agreement for each dispersion measured using the collapse in eq 3. The semiquantitative agreement is reasonable since several factors may contribute to the temperature dependent viscosity. These include a volume fraction dependent Pluronic collapse, a more aggressive temperature dependent collapse, an increasing particle attraction, and instrument limitations for measuring the low absolute viscosities in Figure 6 (particularly because of apparatus used to control evaporation). The initial decrease in the reduced viscosity in each case with increasing temperature suggests a layer collapse consistent with eq 3 that produces the observed transitions.

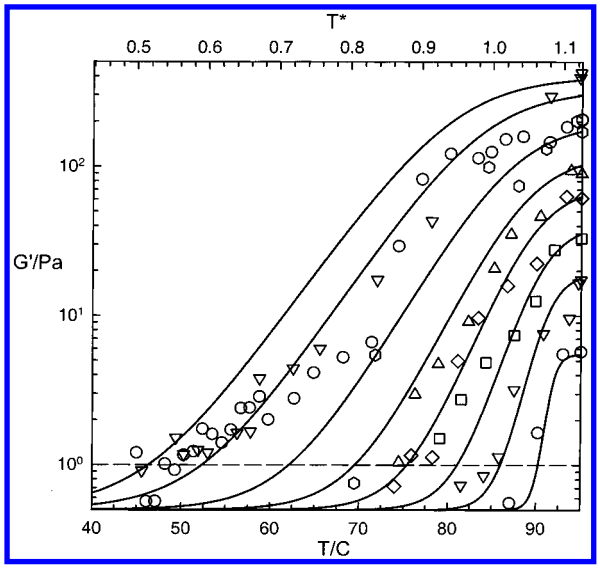

Figure 7. Shear modulus G' (Pa) as a function of temperature (°C) for effective volume fractions (eq 7) of 0.119, 0.162, 0.194, 0.227, 0.2589, 0.302, 0.367, and 0.41. A scale is also shown for the nondimensional temperature T^* (eq 4). Intersection of dashed line (- -) for $G' = 1$ Pa and curve fits (—) (eq 12) indicates values for T_C^* reported in Figure 9.

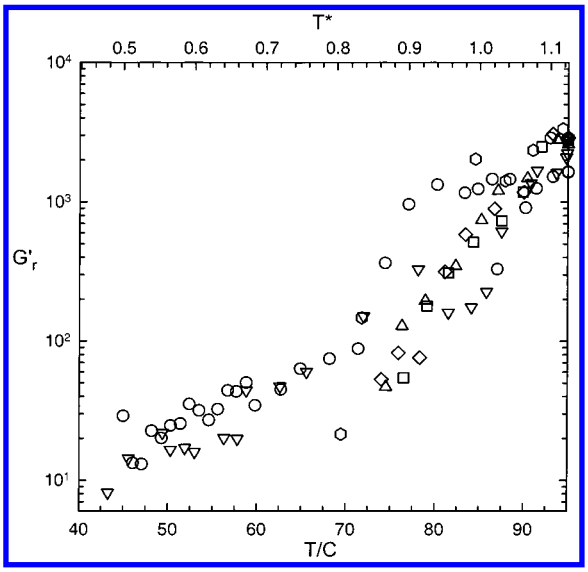

Figure 8. Reduced shear modulus G'_r (eq 13) as a function of temperature (°C) for effective volume fractions (eq 7) of 0.119, 0.162, 0.194, 0.227, 0.2589, 0.302, 0.367, and 0.41. A scale is also shown for the nondimensional temperature T^* (eq 4).

Although there is an obvious volume fraction dependence for the measured fluid−gel transition temperatures in Figure 6, the role of the relatively high (Pe ≈ 1) steady shear must be considered. Particle volume fraction is probed to define the thermodynamic criteria that determine phase behavior in PS/Pluronic dispersions, but applied shear may be expected to mechanically perturb Brownian particle interactions and phase transitions. The absence of appreciable shear thinning for Pe = 0.1−5 in Figure 4 indicates that weak particle interactions are likely to be perturbed from Brownian conditions. To address the effect of shear on the observed phase behavior, Figure 7 reports the shear storage modulus, G', for the same temperatures and dispersions as in Figures 4−6, except that now an oscillatory low shear rate is used with Pe ≈ 0.1 (ω = 3 Hz). For the Pe ≈ 0.1 conditions probed in

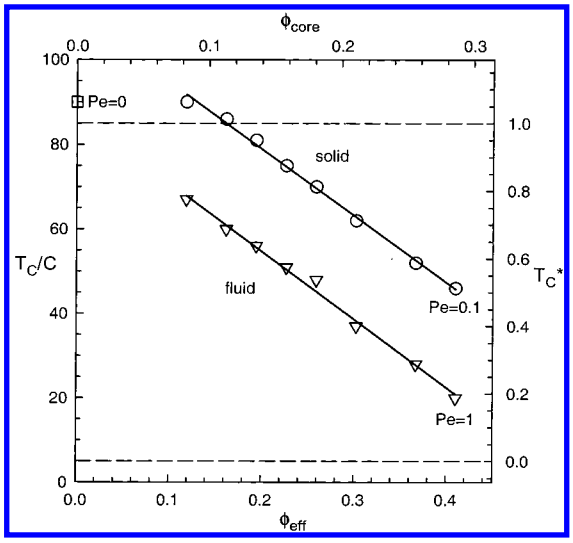

Figure 9. Fluid−gel temperature data T_C (°C) as a function of effective volume fraction for Pe = 0.1 (○), Pe = 1 (▽), and Pe = 0 (□). Scales are also shown for the nondimensional temperature T_C* (eq 4) and the core particle volume fraction.

Figure 7, the mechanical effects on the thermodynamic phase behavior are less than for the Pe ≈ 1 conditions in Figure 6.

These measurements initially indicate a viscous fluid response at 25 °C consistent with Figures 4 and 5 and expected for polymerically stabilized dispersions with $\phi_{eff} < 0.45$.[33] With increasing temperature and interparticle attraction, the data in Figure 7 indicate a unique fluid−gel transition temperature for each volume fraction tested. These transitions were reversible similar to the steady shear transitions in Figure 6. Equilibrium frequency spectra were not measured as a function of temperature in this study, but thermoreversible colloidal gel points determined from a crossover in the storage and loss modulii have been shown to occur over a narrow 0.2 °C range.[34] Empirical curve fits in Figure 7 given by eq 12 were obtained from curve fits to each volume fraction data set and then a regression of the curve fit coefficients as a function of volume fraction. The fluid−gel temperature for each volume fraction are summarized in Figure 9 and are simply interpreted to occur for $G'(T)_{fit} \approx 1$ Pa using eq 12.

$$\frac{G'_{fit}(T,\phi)}{Pa} = 1 + m(\phi)\left[1 + \exp\left(\frac{\tau(\phi) - T/K}{\Delta(\phi)}\right)\right]^{-1}$$

$$m(\phi) = \frac{630}{[1 + \exp(3\phi)^{-4.4}]} \quad \Delta(\phi) = \frac{5.8}{[1 + \exp(5\phi)^{-3.3}]}$$

$$\tau(\phi) = 363 - 200\phi^3 \quad (12)$$

The continued evolution of G' at temperatures above the fluid−gel transition temperatures in Figure 7 suggests a continued increase in particle attraction. Figure 8 reports the modulii measured in Figure 7 as $G'_r(T)$ from eq 13 using scaling suggested for weakly flocculated dispersions.[35] Equation 13 includes the maximum interparticle attractive force, $F_{max}(T)$, the effective particle size, $a_{eff}(T)$, and the effective volume fraction, ϕ_{eff}, at 25 °C. The maximum interparticle attractive force as function of temperature is taken to be the derivative of the van der Waals attraction term in eq 1 evaluated at the minimum formed by the layers in contact at $2\delta(T)$. The Pluronic layer collapse is unimportant for the effective particle size and volume fraction terms in eq 13 and is not included, but is the dominant effect in the $F_{max}(T)$ term.

$$G'_r(T) = \frac{G'(T)a_{eff}^2}{F_{max}(T)\phi_{eff}^{3.7}} = \frac{G'(T)a_{eff}^2}{\left.\frac{\partial E_{vdW}}{\partial r}\right|_{2\delta(T)}\phi_{eff}^{3.7}} \quad (13)$$

The modulii at $G'(T^* = 1.05)$ were fit by scaling ϕ_{eff} to the 3.7 power, which reasonably collapses the data at all volume fractions and temperatures onto a single trend. The $\phi_{eff}^{3.7}$ scaling has been suggested for fractal particle networks created by diffusion-limited aggregation kinetics,[36] which are the kinetics measured for PS/Pluronic dispersions.[19,20] When scaling G' with the maximum attractive force as described in eq 13 and neglecting the Pluronic dielectric properties, the remaining temperature-dependent trend in Figure 8 suggests that a more aggressive increase in interparticle attraction is required. Using eq 1 and ignoring Pluronic properties predicts less than $1kT$ of interparticle attraction for $T^* < 0.9$, which makes it unsurprising that $F_{max}(T)$ does not account for the temperature trend in Figure 8. A greater increase in particle attraction as a function of temperature would better explain the evolution of G' and the occurrence of the observed fluid−gel transition.

The fluid−gel transition data determined in Figures 6 and 7 are summarized in a $T - \phi$ diagram in Figure 9 for both shear conditions with regression lines given by eq 14. The data in Figure 9 display several trends: (1) T_C for $\phi_{eff} = 0.12$, Pe ≈ 0.1 is identical with $T_C = 90$ °C for dilute, Brownian conditions; (2) T_C obtained by extrapolating the Pe ≈ 1 data to infinite dilution is close to $T_C = 90$ °C for dilute, Brownian conditions; (3) $T_C = 20$ °C for $\phi_{eff} = 0.41$ for the Pe ≈ 1 condition is consistent with the general observation that a "fluid" phase with a near hard sphere viscosity could not be prepared for $\phi_{eff} > 0.41$ at any temperature or solvent condition, and (4) the volume fraction dependence of T_C is similar for both shear conditions in terms of the fitted slopes in eq 14, but the absolute temperature is shifted to "better" solvent conditions by 24 °C for Pe ≈ 1 compared with the Pe ≈ 0.1 case.

$$T^*_C(\phi_{eff}, Pe) \equiv \frac{T_C(\phi_{eff}, Pe) - \Theta_L}{\Theta_H - \Theta_L} = \begin{cases} 1.33 - 1.98\phi_{eff}, & Pe = 0.1 \\ 1.03 - 2.01\phi_{eff}, & Pe = 1 \end{cases} \quad (14)$$

The form of eq 14 suggests that mechanical effects due to shear are superimposed on thermodynamic effects due to temperature and particle volume fraction, and can therefore be interpreted independently. The Pe ≈ 1 steady shear shifts the transition to more favorable solvent conditions than the Pe ≈ 0.1 oscillatory shear case, which suggests shear unfavorably affects the adsorbed polymeric interaction. The mechanism by which the shear rate (Pe) affects the fluid−gel transition is not obvious, although it is reasonable that an applied stress can critically affect Brownian particle interactions near a thermodynamic phase boundary. The oscillatory experiments with Pe ≈ 0.1 measures the linear viscoelastic response indicating dispersion microstructure and particle interactions are

(33) Raynaud, L.; Ernst, B.; Verge, C.; Mewis, J. *J. Colloid Interface Sci.* **1996**, *181*, 11.
(34) Rueb, C. J.; Zukoski, C. F. . *Rheol.* **1998**, *42*, 1451.
(35) Buscall, R.; McGowan, I. J.; Mumme-Young, C. A. *Faraday Discuss. Chem. Soc.* **1990**, *1990*, 115.
(36) Buscall, R.; Mills, P. D. A.; Goodwin, J. W.; Lawson, D. W. *J. Chem. Soc., Faraday Trans. 1* **1988**, *84*, 4249.

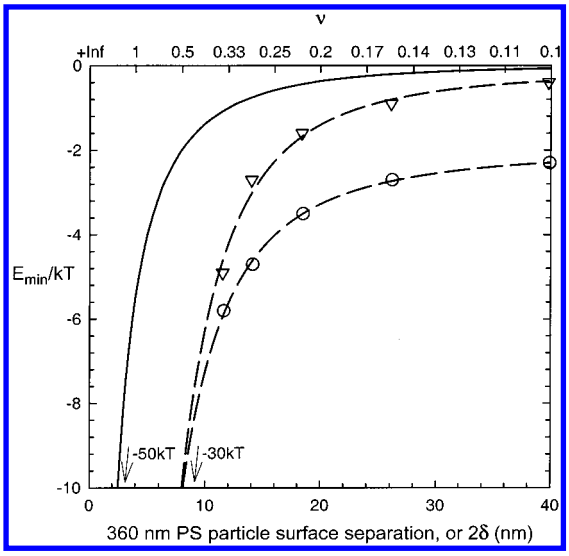

Figure 10. The attraction at the minimum between PS with Pluronic layers having water properties (—), layers modeled as uniform films with average dielectric properties from eq 15 (○), layers modeled as nonuniform films with dielectric properties from eqs 1, 15−17 (s) as a function of 360 nm PS particle surface separation, or 2δ (nm). Curve fits (- -) for the film data are shown to guide the eye. A scale is also shown for the average polymer concentration ν (eq 5).

not significantly altered by the applied shear. To consider volume fraction effects, it is assumed that the Pe $\approx$ 0.1 case in Figure 9 is representative of unperturbed PS/Pluronic dispersion thermodynamic phase behavior.

The Pe $\approx$ 0.1 fluid−gel transition data in Figure 9 indicate significant interparticle attraction for good solvent conditions with $T^* \ll 1$. Although it is possible to interpret the aggregation at $T^* = 1.05$ in Figure 3 solely in terms of a polymeric "mixing" attraction, the fluid−gel transition measured between $0.5 < T^* < 0.9$ in Figure 9 occurs for good solvent conditions where molecular polymeric attraction is not expected. To explain the $T - \phi$ dependence of the fluid−gel transition shown in Figure 10, it is necessary to consider a source of attraction other than polymer mixing. Because physisorbed polymer is used in this study, it is critical to address any apparent role of Pluronic desorption for interpreting the results in Figure 9. For shear rates up to 10^4 s^{-1}, neutron reflectivity measurements of physisorbed block copolymers have not detected desorption at any solvent condition. In fact, these studies report adsorbed polymer density profiles that are unchanged by shear in good solvents,[37] and a slight shear enhanced layer collapse for poor solvents.[38] It is also important to note that $T - \phi$ phase behavior similar to the PS/Pluronic behavior in Figure 9 has been observed for many grafted particle dispersions,[39−45] and in particular for dispersions of PS particles with *grafted* PEO with $a/\delta \approx 5-15$ and $\Gamma = 1.5$ mg/m^2.[41] These analogous results for PS with grafted PEO and PS with adsorbed Pluronic in Figure 9 suggest no obvious role for Pluronic desorption in the observed phase behavior. Finally, desorption was not evident in any of the direct particle measurements with TIRM, and the reversible nature of PS/Pluronic phase transitions are inconsistent with desorption. Assuming desorption is unimportant and knowing that polymeric mixing attraction is not expected for $T_C^* = 0.5-1$, it is essential to quantify the continuum polymeric van der Waals attraction to interpret the observed phase behavior in Figure 9.

Role of Pluronic Continuum van der Waals in PS/Pluronic Phase Behavior ($a/\delta_0 = 4-500$, $T = 25-90$ °C, $\phi \rightarrow 0-\phi = 0.4$, Pe $= 0-1$). This section presents two theories relevant to predicting a solvent quality dependent continuum polymeric van der Waals attraction. The solid line in Figure 10 shows van der Waals attraction between two bare 360 nm PS particles as calculated from eq 1 (ignoring Pluronic properties).[18] This is the equivalent of the minimum depth for two hard wall layers in contact as a function of $2\delta(T)$. The circles shown in Figure 10 indicate the depth of minima formed between Pluronic layers modeled as "uniform" PEO/water films with thicknesses and densities given by Equs. 3 and 5. The retarded interaction of half-spaces with uniform films is calculated by replacing $A_{121}(l)$ with $A_{12321}(l)$ in eq 1 as described elsewhere.[18] Experimentally measured PEO/water dielectric properties for including the adsorbed F108 Pluronic layer in eq 1 are given by eq 15 and described in the Appendix. It should be noted that the PEO/water properties in eq 15, as well as those used for PS and water, are assumed to be independent of temperature since the static terms are completely screened by 0.5 M NaCl.[46] The upside down triangles indicate the depth of the minima formed between Pluronic layers modeled as "nonuniform" films. These points were calculated by replacing the van der Waals term in eq 1 with eq 16, which is described in the 1975 paper by Parsegian, et al.[8] The nonuniform dielectric profile used in eq 16 is given by eq 17 with a parabolic form that mimics a polymer brush density profile.[47] All minima depth are reported for 0.5 nm Pluronic layer separation, which is typical for predicting adhesion energies and avoiding the artificial contact singularity in these continuum theories.[48] Although the solid curve in Figure 10 is the PS van der Waals attraction as a function of surface separation, the dashed curves represent the attractive energy *minima* for layers in contact as a function of layer thickness and are *not* separation dependent van der Waals curves. Using the film models in eq 1 and eq 16, a unique separation dependent van der Waals curve is obtained for each discrete Pluronic thickness, although all calculated curves are close to the dashed curves.

$$\epsilon_{PL}(i\xi_n,\nu) = 1 + C_{uv}(\nu)[1 + [\xi_n/\omega_{uv}]^2]^{-1} \qquad (15)$$

$$C_{uv}(\nu) = 0.762 + 0.4165 \times 10^{-3}\nu,$$

$$\omega_{uv} = 1.90 \times 10^{16}\ \text{rad/s}$$

(37) Baker, S. M.; Smith, G. S.; Anastassopoulos, D. L.; Toprakcioglu, C.; Vradis, A. A.; Bucknall, D. G. *Macromolecules* **2000**, *33*, 1120.
(38) Baker, S. M.; Callahan, A.; Smith, G. S.; Toprakcioglu, C.; Vradis, A. A. *Phys. B* **1998**, *241−243*, 1041.
(39) Everett, D. H.; Stageman, J. F. *Faraday Discuss. Chem. Soc.* **1978**, *65*, 230.
(40) Everett, D. H.; Stageman, J. F. *Colloid Polym. Sci.* **1977**, *255*, 293.
(41) Cowell, C.; Vincent, B. *J. Colloid Interface Sci.* **1982**, *87*, 518.
(42) Edwards, J.; Everett, D. H.; OSullivan, T.; Pangalou, I.; Vincent, B. *J. Chem. Soc., Faraday Trans. 1* **1984**, *80*, 2599.
(43) Rouw, P. W.; Vrij, A.; Kruif, C. G. d. *Prog. Colloid Polym. Sci.* **1988**, *76*, 1.
(44) Chen, M.; Russel, W. B. *J. Colloid Interface Sci.* **1991**, *141*, 564.
(45) Grant, M. C.; Russel, W. B. *Phys. Rev. E* **1993**, *47*, 2606.
(46) Parsegian, V. A. In *Physical Chemistry: Enriching Topics from Colloid and Surface Science*; Mysels, K. J., Ed.; Theorex: La Jolla, CA, 1975; p 27.
(47) Fleer, G. J.; Stuart, M. A. C.; Scheutjens, J. M. H. M.; Cosgrove, T.; Vincent, B. *Polymers at Interfaces*; Chapman & Hall: New York, 1993.
(48) Langbein, D. *van der Waals Attraction*; Springer-Verlag: Berlin, 1974; Vol. 72.

$$E(h,a,\delta,T) = -\frac{\hbar}{32\pi}\int_0^\infty d\omega \int_0^{a+\delta} dr_1 \frac{d \ln \epsilon(r_1,\omega)}{r_1} \times \int_0^{a+\delta} dr_2 \frac{d \ln \epsilon(r_2,\omega)}{r_2} G(r_1,r_2) \quad (16)$$

$$\epsilon_{PL}(i\xi_n,\nu,\delta,r) = \epsilon_{PL}(i\xi_n,\nu) - [\epsilon_{PL}(i\xi_n,\nu) - \epsilon_{H2O}(i\xi_n)](r/\delta)^2 \quad (17)$$

Before discussing implications of the predicted attraction in Figure 10 for phase behavior in Figure 9, it should be noted that both film models have limitations for accurately modeling the PS/Pluronic potential, although these limitations are somewhat complementary. The uniform film model rigorously considers retardation, but approximates the Pluronic density profile. In contrast, the nonuniform film model does not include retardation, but allows for an arbitrary density profile. Both models satisfy critical theoretical limits: (1) they predict stronger attraction at Pluronic contact than bare PS attraction at the same separation, (2) but the also predict weaker attraction at Pluronic contact compared to bare PS contact. For a total Pluronic collapse to $\delta \rightarrow \Gamma/\rho_{PEO}$ and $\nu \rightarrow 1$, the models converge to nearly the same value with $E_{min} = -33kT$ for nonuniform films and $E_{min} = -27kT$ for uniform films. This convergence is expected since the uniform film more accurately represents the Pluronic density profile, and retardation is less important for small δ in the unretarded nonuniform film model. For an incomplete Pluronic collapse, both models over predict attraction since the nonuniform film model neglects retardation and the uniform film model does not accurately describe the Pluronic profile. However, in contrast to the uniform film, the nonuniform film model predicts attraction increasingly similar to bare PS attraction as the films become thicker and more dilute in polymer, which is important for predicting stability in polymerically stabilized dispersions. Although the uniform film model is useful in the limit of a total Pluronic collapse, the nonuniform film model is more accurate for all layer thicknesses and extents of solvation. Except for neglecting retardation, the nonuniform film appears more promising than the uniform film model for accurately describing polymeric van der Waals for all solvent conditions and a/δ_0.

The PS/Pluronic composite particle van der Waals attraction in Figure 10 predicted by the nonuniform film model is sufficient to cause the phase transitions in Figure 9 for good solvent conditions when the core PS particle attraction alone is not enough. The nonuniform film model in conjunction with the Pluronic collapse in eq 3 predicts attraction of $\sim 1kT$ at 45 °C, $\sim 3kT$ at 70 °C, and $\sim 5\ kT$ at 85 °C, while the bare 360 nm PS core particle attraction with the same Pluronic collapse produces less than $1kT$ of attraction up to 85 °C. In the case of a more aggressive layer collapse that might be expected in concentrated dispersions,[28] the attraction would increase to even greater magnitudes with decreasing solvent quality. In general, anything causing a Pluronic layer collapse, or an increased density of PEO dielectric properties, will result in an increase in the Pluronic continuum van der Waals contribution. For a total Pluronic layer collapse, both predictions in Figure 10 indicate a net attraction around $-30kT$, which suggests the possibility of producing conditions for thick polymer layer dispersions that result in irreversible aggregation and gelation. Given that attractive interactions between $1kT$ and $5kT$ are critical for phase behavior, both film models suggest the net composite particle continuum van der Waals attraction is critical for understanding polymerically stabilized dispersion phase behavior.

In addition to predicting attraction sufficient to cause the phase behavior in Figures 3 and 9 for particles with relatively thick polymer layers, the nonuniform film model also accurately predicts attraction for particles with thin polymer layers. While continuum polymeric attraction controls temperature-dependent phase behavior of thick polymer layer dispersions with $a/\delta_0 < 40$ in Figures 3−9, it is unimportant for the thin polymer layer dispersions with $a/\delta_0 > 40$ in Figure 3. This is apparent in Figures 1 and 3, since eq 1 accurately predicts attraction for the thin polymer cases by ignoring the Pluronic dielectric properties. Since the nonuniform film model in eq 16 predicts attraction approaching the bare PS particle attraction predicted by eq 1 for the case of thin layers, it is expected to be accurate for all relative particle sizes and layer thicknesses. However, the nonuniform film model neglects retardation and over predicts attraction for particles with large absolute radii. To accurately predict the phase behavior for all *absolute* PS particle radii and all *relative* values of a/δ_0 measured in this paper, the nonuniform film model must include the effect of retardation.

It is beyond the scope of the present paper to explore corrections to the nonuniform film model to account for the effect of retardation. Since this paper does not include quantitative predictions of the results in Figure 9, it is not obvious how including retardation in eqs 1 and 16 affects the measured phase behavior. A manuscript is in preparation which uses a Casimir−Polder type retardation correction and the adhesive sphere model to construct a theoretical phase diagram for comparison with the measurements in Figure 9. Comparison of the adhesive sphere $T - \phi$ diagram and the retarded nonuniform film model with no adjustable parameters will provide a link between the microscopic pair potential and macroscopic phase behavior.

Conclusions

The measurements reported here show that for the case where Pluronic layers are much thinner than the PS particle radii, the interaction potential and aggregation behavior are well described by a temperature-dependent polymeric hard wall interaction superimposed on a core particle continuum van der Waals contribution. When the radii of the PS particles are less than 40 times the thickness of the Pluronic layers, the core particle attraction alone does not appear sufficient to explain the phase behavior observed in this paper. Dilute Brownian temperature-dependent aggregation and concentrated fluid−gel measurements of thick polymer layer dispersions suggest a continuum polymeric van der Waals attraction in addition to the core particle attraction. Desorption of the physisorbed Pluronic is considered as a possible source of attraction and the observed phase behavior, but is dismissed in favor of a continuum polymeric van der Waals contribution to the net composite particle attraction. Initial calculations modeling the adsorbed Pluronic as a uniform or nonuniform film suggest the polymeric attraction is sufficient to cause the observed phase behavior. Future work will compare the observed phase behavior in this paper with a retarded nonuniform film model and predicted $T - \phi$ phase behavior. These measurements indicate the quantitative links between microscopic measurements of the interparticle potential and macroscopic phase behavior and rheological transitions in polymerically stabilized systems.

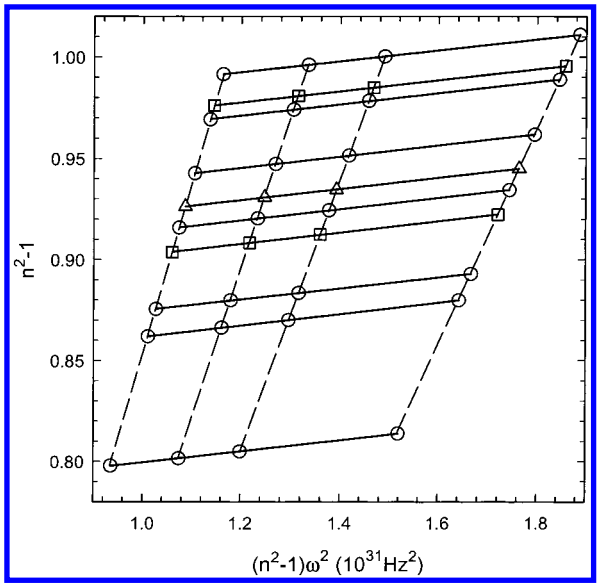

Figure 11. Cauchy plot of $(n^2 - 1)$ plotted against $(n^2 - 1)\omega^2$ for 8000 MW PEO (○) solutions with $\nu = 0.05$, 0.20, 0.26, 0.33, 0.39, 0.45, and 0.50; 400 MW PEG (□) solution with $\nu = 0.30$ and 0.47, and a F108 Pluronic (△) solution with $\nu = 0.35$. The refractive indices were measured at wavelengths of 436, 488, 515, and 550 nm. The solid curve fit lines (—) are given by eq 18. Dashed curves (- -) are shown to illustrate the consistency of the data.

Acknowledgment. This work was supported by the Australian Research Council and the Particulate Fluids Processing Centre at The University of Melbourne. Refractive indices of PEO, PEG, and Pluronic solutions were measured by Mr. Mark Kimmel at Carnegie Mellon University.

Appendix: Dielectric Spectrum of PEO/Water Layer

This appendix explains how parameters representing the Pluronic layer dielectric properties in eq 15 were obtained from aqueous solution refractive index data using the "Cauchy plot" method described by Hough and White.[11] For dielectric spectra dominated by a single UV absorption peak, eq 18 can be used to give the refractive index as a function of frequency. Since the Pluronic layer can be described by a PEO density profile normal to the PS particle surface, the parameters in eq 18 are given as function of PEO/water concentration. For molecules such as water and PEO that have permanent dipole moments, the dielectric constant is also typically included, but the 0.5 M NaCl used in these experiments completely screens this term in the eq 1 so it is not included here.

To construct a Cauchy plot, a differential refractometer was used to measure the refractive index of PEO, PEG, and Pluronic solutions between $\nu = 0.05-0.5$ for visible wavelengths of 436, 488, 515, and 550 nm. The solutions used were $\nu = 0.05$, 0.20, 0.26, 0.33, 0.39, 0.45, and 0.50 for 8000 MW PEO and $\nu = 0.30$ and 0.47 for 400 MW PEG, and $\nu = 0.35$ for F108 Pluronic. Figure 11 show a Cauchy plot of $(n^2 - 1)$ plotted against $(n^2 - 1)\omega^2$ for various concentrations of aqueous solutions where ω is the wavelength of light converted to frequency units of Hz. A linear regression to the data in Figure 11 at each concentration produces a linear slope of ω_{uv}^{-2} independent of PEO concentration, and an intercept C_{uv} for each curve that is linearly dependent on PEO concentration. The resulting parameters and spectrum are reported in eq 15.

$$n^2(\omega,\nu) = 1 + \frac{C_{uv}(\nu)}{1 - [\omega/\omega_{uv}(\nu)]^2} \qquad (18)$$

LA0110646